Flame Assisted Chemical Vapour Deposition of NiO hole transport layers for planar perovskite cells

Heather M. Yates [a]*, John L. Hodgkinson[a], Simone M.P. Meroni[b], David Richards[b] and Trystan M. Watson[b]

[a] Materials and Physics Research Centre, University of Salford, Manchester, M5 4WT, UK.; [b] SPECIFIC, Swansea University, Bay Campus, Fabian Way, Crymlyn Burrows, Swansea, SA1 8EN, Wales UK.

*corresponding author: E-mail: H.M.Yates@salford.ac.uk

phone +44 (0)161 295 3115, fax +44 (0)161 295 5575

Abstract

Thin films of polycrystalline NiO were deposited by Flame Assisted Chemical Vapour Deposition, which is an ideal process for in-line, atmospheric pressure deposition of wide area coatings. This, along with the ability to use aqueous salts rather than organic precursors or solvents makes it well suited for industrial integration. To establish the capability of FACVD deposited NiO for use as a low cost, commercially viable option planar perovskite cells were fabricated under ambient conditions. The resulting cells showed the importance of both the flame composition and NiO thickness. A continuous NiO Hole Transport Layer (HTL) was achieved for ca. 36 nm thick film, which showed a maximum higher efficiency of 12.3% over that of the control (11.8%) which used a spin coated HTL. This was mainly driven by the large improvement in the current density from 16.6 mA/cm^2 to 19.0 mA/cm^2.

Keywords: FACVD; CVD; NiO; perovskite; hole transport

1.Introduction

Solid-state organic-inorganic hybrid perovskite solar cells have seen a meteoritic rise in interest since early work [1] in the 1990's on conductive tin halide based organic based perovskites, through the more commonly recognised $CH_3NH_3PbI_3$ (MAPI) in mesoporous TiO_2 with a 3.8% cell efficiency [2], to reported efficiencies of 22.1% (cell size 0.095 cm^2, 19.7% 1 cm^2) for solely perovskite [3] and the recently announced 28% (cell size 1 cm^2) by Oxford PV [4] when combined as a tandem with the already commercially viable Si thin film market. Initially, the most common perovskite cell configuration was n-i-p, which included a sintered mesoporous scaffold layer, typically TiO_2 to aid the electron charge transfer and an expensive complex organic spiro-OMeTAD as the hole transport layer. Inverting the structure to p-i-n removes the need for the scaffold or use of spiro-OMeTAD, opening up to a range of cheaper, more stable inorganic oxides. In addition to reducing the number of fabrication stages and hence a potential reduction in commercial costs.

Use of NiO has been shown to provide an effective hole transporting layer, which removes the issue of TiO_2 instability related to its photocatalytic behaviour on absorption of UV light [5] and provides a solar cell with minimal hysteresis [6]. NiO has been deposited by a range of techniques including sputtering [7], spray pyrolysis [8], spin coating [9, 10] and Aerosol Assisted Chemical Vapour Deposition (AACVD) [11]. Sputtering works well, but it has some disadvantages of inflexibility and high running costs due to the vacuum technology, while spray pyrolysis, spin coating and AACVD all require use organic precursors and/or organic solvents. These as well as being detrimental to the environment can also lead to greater impurity incorporation in the films and hence reduce device quality. Spin coating, while a successful process for small scale batch processing is not scalable and hence lacking suitability for industrial integration. Another draw-back for this process is, in some cases, the need for an extra annealing stage to improve crystallinity [12]. In addition, AACVD and

sputtering generally have relatively low deposition rates. One technique which avoids these problems is the atmospheric pressure technique of Flame Assisted Chemical Vapour Deposition (FACVD). This provides a method to produce either large area batch or in-line coatings, with the added advantage of the ability to use easily available, cheap, aqueous salts, rather than as in AACVD the need for organic solvents. The ability to deposit films without environmentally damaging organic solvents helps reduce the extent of film contamination. FACVD is capable of high deposition rates, another consideration for commercial integration. For example, we have previously shown deposition rates of 140 nm min^{-1} for silver [13] as opposed to 22 nm min^{-1} AACVD [14] and up to 202 nm min^{-1} for copper oxides [15] opposed to a maximum of 17 nm min^{-1} AACVD [16]. Although, all these are relatively high in comparison to deposition rates possible by atomic layer deposition with for example 0.34 nm/cycle for NiO deposition [17] or 6 nm min^{-1} for magnetron sputtering [18]. In contrast, within some reported literature there is also the need for slow deposition processes to enable deposition of pin-hole free ultra-thin layers utilising AACVD with deposition rates deliberately brought down to those of atomic layer deposition [19].

Most commonly, the NiO layer in a planar perovskite device is deposited via spin coating a sol-gel system, which employs a precursor solution such as nickel acetate tetrahydrate, which is then annealed for at least 30 minutes at temperatures above 300 ^{o}C [20, 21]. One added advantage of FACVD is that the process naturally produces polycrystalline thin films, so dispensing with the need for an annealing stage. Efficiencies have now reached up to 18.15% using this device architecture (ITO/NiO_x/PSK/PCBM/BCP), owing to the high quality perovskite film achievable when deposited under low humidity conditions in a glovebox [22]. However, highly crystalline perovskite films fabricated in ambient conditions using an anti-solvent have made high efficiency NiO based planar solar cells (PSC) achievable. Troughton et al [20] fabricated PSCs with power conversion efficiencies (PCE) of up to 14.5% in air using this method, as well as demonstrating a 13.5 cm^2 module achieving efficiencies in

excess of 10%. Although this cell fabrication method provides highly crystalline and effective NiO hole-transport layers, it is not easily scalable; therefore, a large scale deposition method such as FACVD is required.

To produce a truly commercially viable PSC all the individual layers must be capable of being deposited over large areas. Control of the perovskite morphology during scale-up has proved to be particularly challenging and now being surmounted by use of techniques such as slot-die [23], spray coating [24] and screen printing [25]. Slot die with its potential for high coating line speeds could be particularly compatible with FACVD to bring the commercialisation of low cost, efficient PSC's closer.

In this paper we describe the use of a flame type atmospheric pressure, in-line technique to deposit polycrystalline NiO. Although this method has previously been reported by us for a range of mainly oxides, its use for NiO deposition has been very limited. Recently, we utilised the process to produce porous NiO films as hole transport layers to enhance the efficiency of mesoporous carbon perovskite cells [26]. This has now been extended to demonstrate FACVD capabilities to deposit pin-hole free continuous thin films within another type of perovskite solar cell. The effect of deposition parameters on the morphology and structure of the deposited NiO are discussed, along with the effects on resistivity and structure of the transparent conducting electrode of indium tin oxide (ITO). Finally, we show the potential to use FACVD deposited NiO as a compact hole transport layer (HTL) within a planar perovskite solar cell (P-PSC).

2.Experimental

2.1 Deposition of NiO - The NiO films were deposited via FACVD, using a 0.05M nickel nitrate solution prepared from nickel nitrate hexahydrate (99.999% Sigma Aldrich). An ultrasonic nebuliser, along with a nitrogen carrier gas flow of 2 L min^{-1} was used to deliver the precursor aerosol to the burner head. Oxygen (0.6 L min^{-1}), along with the Ni precursor

was added to the combustion gases of propane and air upstream of the burner head. Addition of oxygen was previously found by us to improve reproducibility and enhance film crystallinity [27]. Two flow ratios of combustion gases were used 0.8 L min^{-1} propane/ 22 L min^{-1} air for a 'lean flame' and propane 1 L min^{-1} / 20 L min^{-1} air for a 'standard' flame. The susceptor set temperature was 400°C and was translated (10 mm s^{-1}) under the flame to mimic an online process. The number of passes of the substrate under the flame was varied from 12 to 50. Borosilicate glass or ITO coated glass were used as the substrates.

2.1 Cell Fabrication – The method reported here is that previously used by us [20] to obtain high quality perovskite cells under controlled ambient conditions. For the P-PSC, on a ITO/glass substrate, layers of NiO, perovskite, PCBM, PCB and silver were deposited as follows: a 0.2 M solution of nickel acetate tetrahydrate (Sigma Aldrich) (50 mg/ml) in 2-methoxyethanol (Sigma Aldrich) with the addiction of 12 µl/ml of ethanolamine (Sigma Aldrich) was spin coated onto the substrate at 2000 rpm for 30 seconds and then annealed on a hotplate for 30 minutes at 300 ^{o}C. The perovskite precursor solution was made in the glove box by dissolving 576 mg/ml PbI_2 (TCI) and 199 mg/ml MAI (Dyesol) in a 4:1 ratio of DMF:DMSO (Sigma Aldrich). All subsequent steps were carried out in the open laboratory environment. The solution was then was deposited onto the substrate and spun at 4000 rpm. With 10 seconds left on the spinning cycle, 100 µl of ethyl acetate was dropped onto the spinning substrate. After spinning, samples were placed on a hot plate at 60 ^{o}C, and then annealed at 100 ^{o}C for 10 minutes. A solution of 99.5% PC60BM (Solenne BV) was produced by dissolving 40 mg/ml PCBM in chlorobenzene. The solution was then spun on top of the perovskite layer at 3000 rpm for 60 seconds, with no further drying. 0.5 mg/ml of bathocuproine was dissolved in ethanol and left to stir overnight on a hot plate at 60 ^{o}C. The solution was spun on top of the PCBM layer at 7000 rpm with no further drying. A silver top contact was evaporated on the top of the device.

2.3 Characterisation

A scanning electron microscope (FEI Quanta 250 ESEM) provided surface and cross-sectional images. ImageJ software was used to extract feature size and separation [28]. The surface roughness was obtained from atomic force microscopy (NanoScope IIIa, Digital Inst. Ltd.). X-ray diffraction (Siemens D5000) with a Cu Kα source was used for structural characterisation of the films. Crystallite size was calculated from the Scherrer equation [29]. The resistivity of the ITO was measured using a Jandel Universal four point probe. A uv/visible spectrophotometer (Aquila nkd 8000) was used to obtain transmission and reflection measurements between 400 - 1000 nm at an incident angle of 30° using p polarization.

A Thermo Fisher Scientific NEXSA X-ray photoelectron spectrometer was used to determine surface chemical composition. A micro-focused monochromatic Al x-ray source (72 W) scanned samples over an area of approximately 400 microns. Data was recorded at pass energies of 200 eV for survey scans and 50 eV for high resolution scan with 1 eV and 0.1 eV step sizes respectively. Charge neutralisation of the sample was achieved using a combination of both low energy electrons and argon ions. CasaXPS was used for data analysis using a Shirley type background and Scofield cross sections, with an energy dependence of -0.6. The scans were calibrated using the C1s binding energy of 285 eV.

Current-voltage testing of devices was performed using a class AAA solar simulator (Newport Oriel Sol3A) as a light source calibrated to one AM1.5 sun equivalent intensity using a reference cell fitted with a KG5 filter (Newport Oriel 91150-KG5). Current-voltage curves, in reverse and forward scan directions, were collected using a Keithley 2400 source measure unit between bias of 1.1 and -0.1 V at a scan rate of 0.15 V s^{-1}. Device pixel size was 0.15 cm^2.

3.Results and Discussion

3.1 Material properties - As we have previously reported [13] FACVD deposition leads initially to island growth, before eventually coalescing and forming a complete thin film. Figure 1 established that this process also occurred for NiO deposition with initially small separate particles which gradually grow and merge. The film with the greatest number of passes of the coater head over the substrate (Fig.1c) can be seen to consist of both large particles on the surface with smaller ones between, which were all confirmed to be NiO by EDAX (Fig.S1). This type of island growth is known as the Volmer Weber growth mode [30] where there is a gradual merging of islands to decrease island density resulting in local clearing of the substrate where further nucleation can take place. This occurs while the height and size of remaining of the islands increases. To look at this in more detail the average island size and separation was extracted from the SEM images using ImageJ software. Figure 2 establishes that this process also takes place for the NiO FACVD deposition with a gradual increase in island size with increased separation. Looking more closely it can be seen that initially there is very little change in island size with increasing number of passes of the substrate under the coater head. This is typical of the Volmer Weber growth mode where the depositing atoms bond more strongly to each other than the substrate. This implies that the islands initially are increasing in height rather than length.

To calculate the static deposition rate under the standard flame a relatively thick film was chosen so that the film height was that of a film, not individual islands of growth. In addition, due to the limited resolution of the SEM a thicker film reduced the errors in measuring thickness. Based on a film of 65 nm (σ = 11 nm) the static equivalent deposition rate (propane: air 1:20 L min^{-1}) was calculated to be 40 nm min^{-1}, (σ = 7 nm min^{-1}). As suggested later in this paper a continuous film was achieved by 50 passes under a reduced propane lean flame with a thickness of 36 nm (σ = 6 nm), which equated to a static rate of 22

nm min^{-1} (σ = 4 nm min^{-1}). The lower deposition rate of the NiO derived from the lean flame modified the surface morphology. As can be seen in figure 1 when comparing two films of similar thickness the lean flame derived NiO (Fig.1d) had a more compact surface with smaller features than the standard flame sample (Fig.1b). Although, lower than we have previously reported for other materials by FACVD, which generally used a higher proportion of propane, it is comparable than that reported for NiO deposition via AACVD [11] with the added advantage of an aqueous, rather than organic solvents. The deposition rate from Sialvi et al [11] was calculated from the SEM data provided on the thickness of the combined F-doped SnO_2 (NSG TEC C15 at 350 nm) and NiO deposition giving a rate of 19 nm min^{-1} based on NiO films up to 280 nm thick. Increased FACVD deposition rate via changes to deposition parameters such as delivery rate, precursor concentration, flame height [31] or translation speed [32] could help increase the deposition rate.

It is important that the NiO film can be deposited without damage to the underlying layers. In this case the ITO front electrode. XRD established that ITO has the polycrystalline structure of In_2O_3 (JCPDS 06-0416) shifted approximately 0.2° lower due to Sn doping. Checks on the effect of the flame on ITO showed the importance of using a lean (lower propane flow) flame. As can be seen in figure 3 50 passes of a standard flame led to complete loss of any crystallinity and destruction of the ITO. The surface of the ITO coated glass became opaque and grey in colour unlike the surrounding uncoated glass which stayed transparent. It is very likely that the flame reduced the oxide to indium metal and then due to its relatively low melting point (157 °C) partial evaporation. In addition, the remaining film was highly electrically resistant. Similar tests with ITO under lean flame, less reducing conditions (50 passes under flame) established no obvious increase in crystallite size from 20 nm to 24 nm for the (400) orientation at 35°. However, on addition of NiO the change in ITO crystallite size is negligible. Even with 50 passes of the lean flame the ITO diffraction pattern does not change, nor do samples showed any peak related to In metal. The only overlap is for a small

diffraction peak at 33^{o}, which is present in both oxide and metal, but does not change in intensity on FACVD treatment, so is almost certainly due to the oxide.

Deposition directly on glass with a lean flame established polycrystalline cubic NiO (JCPDS-47-1049) with diffraction signals at 37.5^{o} (111) and 43.5^{o} (200). Unambiguous assignment of NiO on ITO is difficult as both the ITO (411) and (422) lie in the positions for the NiO ((111) and (200) respectively (Fig.4). Together with the relative weakness of the NiO signals. However, as would be expected, there is a small reduction in ITO signal intensity as more NiO is added. This is particularly obvious when looking at the relative intensities of the signals at 37.5^{o} relative to 37.9 ^{o}. Therefore, the increasing signal at 37.5^{o} is assigned to NiO (111) and the deceasing signal at 37.9 ^{o} to ITO (411).

A comparison of surface profiles (AFM, SEM) before and after 50 passes under the lean flame treatment (no NiO) showed no obvious differences, re-enforcing the lack of structural change. Although the roughness of the ITO was marginally increased from 1.0 nm (σ=0.1 nm) to 1.6 nm (σ=0.1 nm). Adversely, there was a large increase in sheet resistance from 9.4 Ω/□ (σ=0.6 Ω/□) to 103 Ω/□ along with a small reduction in average transmission (86% to 84%) between 400 nm and 1000 nm. With the addition of between 12 and 50 passes of NiO the sheet resistance results were not as severe and showed increases to 31 Ω/□ (σ=10 Ω/□). This, although high, was still much lower than that of the ITO directly treated with the flame. The increase in sheet resistance will be due to both the gradual covering of the ITO surface and damage from the flame. That the values recorded are much lower than that of the flame only sample suggest that the NiO layer helped protect the underlying layer as it was no-longer directly in view of the flame.

The structure of deposited NiO is clear when deposited directly on glass (see Fig.5c), but there was limited change to the ITO morphology on addition of NiO, even at 50 passes as shown in the SEM comparison in figure 5. The surface of the ITO film is very smooth (R_q ~1

nm, R_p 3 nm, R_t 9 nm), but still showed strong characteristic features on deposition of what on glass was a continuous NiO film (R_q 1.8 nm, σ = 0.1 nm). Addition of NiO onto the ITO substrate (R_q 3.1 nm, σ = 0.6 nm) made only a limited change to the surface roughness. The roughness value for NiO on ITO is in line with those reported previously by Liu et al [6] of 3.4 nm for a comparable thickness film (30 nm thick) and Jung et al [12] of 4.5 nm (50 nm thick). There are some larger spherical features, which could be NiO powder from a homogeneous reaction, but these would not be enough to have provided both XRD and XPS evidence that NiO was present and coated over the ITO substrate.

AFM surface images (Fig.6a-c) compare the morphology of the ITO substrate and simultaneously deposited films of NiO directly on glass and the ITO substrate. Quantitative analysis of the AFM surface images to produce height histograms (Fig.6d) established that the ITO substrate had a very small range of surface height features, in agreement with its uniformity and low R_q roughness. In contrast once 50 passes of NiO had been deposited directly on glass or ITO the height histogram broadened reflecting the wider variation in feature height in line with the island growth nature of FACVD NiO.

XPS (Fig.7) is a surface sensitive technique so the substantial reduction in the In 3d signal intensity to 13% the original on coating with 8 passes NiO to 3% with 12 passes and 1.3 % by 50 passes established that the ITO must be mainly under the NiO. The In 3d signal was asymmetric for both as provided and ITO subjected to 50 passes under the flame (no NiO) and fitted two resolved $3d_{5/2}$ peaks at 444.6 eV and 443.9 eV. The samples coated with NiO showed a gradual shift towards the lower BE as the number of NiO coating passes increased, reflecting the change in intensity ratio between these two fitted peaks (See graph in Fig.7). The position of this peak for as provided and ITO treated under 50 passes of a lean flame (no NiO) is shown at the ’60 pass’ position. The weak intensity of the In 3d for the NiO coated samples prevented accurate fitting of two distinct peaks. The intensity of the oxide peak

dropped from 67% to 58% on flame treatment, probably due to reduction of some oxide, although either amorphous or of too small a concentration to be detected by XRD. The reported In 3d shift for metal and oxide are 1 eV apart [33], while the difference here is 0.7 eV so possibly affected by the presence of the Sn dopant. Clarke et al [34] assigned In 3d peaks at 444.8 eV and 443.6 eV to the metal oxide and metal respectively. However, in contrast Zhou [35] suggested doping with Sn shifts the In 3d by 1 eV and that of the Sn 3d by 2 eV to higher binding energy, although the values stated, when allowing for a different C 1s reference value are the same as Clarke's which was for an undoped indium oxide sample. In this work the Sn 3d within the ITO is shifted by 0.6 eV relative to a SnO_2 sample.

The Ni 2p signal consisted of 4 main broad peaks (Fig.8) relating to the $2p_{5/2}$ round 854 eV, $2p_{1/2}$ 873 eV and their related satellites at 861 eV and 880 eV respectively, with a splitting of ca. 18.1 eV. The broad nature of the 2p peaks (and a pronounced shoulder) made it difficult to accurately determine their separation. The theoretical value is 17.49 eV [33], but our value was similar to that found by Turgut et al [36] of 18.3 eV. There was no signal which could be fitted to Ni metal at 852.7 eV. These signals can be assigned to nickel oxides, although the exact designation can be difficult due to the complex splitting of Ni 2p which can be resolved into multiple states [37]. The $2p_{3/2}$ was resolved into two peaks at 854.7 eV and 856.6 eV which were assigned to Ni^{2+} and Ni^{3+} in agreement with the literature [38, 39]. However, care is needed as one satellite (seen as a shoulder) coincides with Ni^{3+} at 856.1 eV making definitive assignment difficult [40].

Fitting the Ni 2p and O 1s established that the deposited material was stoichiometric. There was no obvious change in position or relative curve intensities of the Ni 2p from deposition on glass to that on ITO, which helped confirmed that there had been no change in the NiO chemical structure due to the different substrates.

Based on the materials analysis NiO was deposited on ITO substrates under the lean flame as this provided a more compact film of higher crystallinity [26], along with much reduced damage in the ITO substrate. Solar cells were fabricated with these to demonstrate the ability of the FACVD process to produce viable, efficient cells and to assess the effects of NiO thickness.

3.2 Cell performance - Planar MAPI cells were fabricated with a range of FACVD NiO thicknesses, along with a control sample with a spin coated 33 nm thick (σ = 4 nm) NiO HTL. As can be seen in the box plots in figure 9 it was possible to fabricate working cells with NiO layers from 12 to 50 passes of the substrate under the FACVD coating head. The highest cell efficiency was obtained from the 50 pass NiO sample, with a maximum PCE value of 12.3%. This is fractionally higher than that of the optimised control spin coated NiO derived cell of 11.8%. This gain in efficiency relates to the much higher current density, J_{sc} of the FACVD derived cell over that of the control with maximum values of 19.0 mA/cm^2 and 16.6 mA/cm^2 respectively. Both sets of cells showed similarly narrow distributions with average J_{sc} values of 15.67 ± 0.17 mA/cm^2 and 18.41 ± 0.18 mA/cm^2 for the control and 50 pass NiO derived sample respectively. However, the FACVD derived sample has a lower fill factor, FF (63.0%) than that of the control device (72%). All samples (bar the flame treated 'No NiO') gave relatively similar open circuit voltages, V_{oc}, with narrow distributions. This is not too surprising as this value is limited by the bandgap which will be very similar for all samples, hence mainly affected by non-radiative losses and charge transport.

As discussed earlier in this paper, the NiO particles increased in size with the number of passes under the FACVD coating head to around 36 nm for the 50 pass lean flame derived sample. It appears that after 50 passes under the flame, larger particles agglomerate on top of a layer of much smaller particles, leading to an increase in surface area. This increase in surface area is the most likely cause for the increase in current as the perovskite layer will

also have a higher surface area when compared to the other samples. Larger particles in the HTL will also provide a smaller number of grain boundaries, leading to fewer defects in the film, and thus better charge extraction. Comparing the JV curves (Fig.S2) of the control device and best performing FACVD device, there was an increase in series resistance for the FACVD device which led to a drop in FF. This was to be expected as a high sheet resistance of 31 ± 6 Ω was measured for the FACVD device with 50 passes of NiO. An increase in hysteresis was observed for the FACVD device, which suggests that it is not as effective at hole extraction when compared to the control device. The remaining devices showed gradually improving JV curves (Fig.S2) as they progress in increasing NiO thickness from 12 passes through to 50 passes.

As seen in the materials characterisation section addition of NiO shields the ITO from the flame so limiting the damage. This was reflected by the very poor performance of the cells fabricated from the ITO substrate which had been passed under the flame (50 passes) with no NiO addition and then subsequently completed with spin coated NiO as for the control. These are designated 'no NiO' in figure 9 and figure S2. The extremely poor JV curve (Fig.S2e) and hence the reduction in efficiency is most likely due to the increased resistance in the ITO when passed under the flame CVD.

The P-PSC cells on ITO need a compact NiO layer with no pinholes for optimum performance, to prevent shunts. The box plots (Fig.9) clearly show the point at which the AP FACVD NiO layer became continuous with an abrupt jump in values for J_{sc} and the overall efficiency when the number of passes increased from 30 to 50 passes (36 nm thick). An incomplete surface coverage, with pin holes would allow recombination reactions and thus reduce the J_{sc}.

It has previously been reported that the thickness of NiO within the solar cell has a strong effect on device performance. For example, Tang et al [41] reported that for a range of HLT

thicknesses between 30 nm and 170 nm the cell efficiencies varied between 9.1% to 15.4%. The absolute optimum thickness depended on both NiO (structure, particle size, crystallinity) and fabrication (deposition method, choice of precursors). In addition, the absolute efficiency was dependent on the exact composition and thicknesses of the other cell layers [10]. For example, optimum HLT NiO thicknesses have been reported for 10 nm [42], 40 nm [43], 49 nm [10] and 55 nm [41].

In comparing our results to those in the scientific literature care must be taken, as noted earlier the absolute efficiency values depend on the perovskite composition and the thicknesses of the individual layers which make up the cells. Higher efficiencies than ours have been achieved for planar cells which were optimised for other materials and different cell sizes. It is more difficult to fabricate large areas free of defects and pinholes so generally smaller device sizes will have higher apparent PCE [44]. For instance, Yin et al [10] using a F-doped SnO_2 TCO with thicker layers of NiO (49 nm) attained an efficiency of 13.99%, albeit with a thicker layer of perovskite (334 nm opposed to 260 nm) and a much smaller cell size (0.06 cm^2 opposed to 0.15 cm^2), which would help improved efficiency. While Tang et al [41], again using SnO_2:F and a thicker perovskite layer (370 nm), with a slightly smaller cell size (0.12 cm^2) using an optimised NiO thickness of 55 nm obtained 15.47%. Conversely Saranin et al [42] using a much thinner NiO layer (10 nm) reported an average efficiency of 14.82%. This wide range of optimised HLT thicknesses confirms the number of variables and their interlinking within solar cell fabrication to provide a fully optimised device.

Nevertheless, our work established that irrespective of the NiO deposition method (spin coated or FACVD) on identically produced P-PSC the highest efficiencies were obtained for NiO films of similar thickness (33 nm spin coated, 36 nm FACVD). However, the FACVD derived P-PSC have the major advantage of being deposited via a commercially viable process, unlike spin coating and without the need to use organic solvents or an additional annealing stage. In addition, in this study, with a much-improved current density. The

FACVD HTL derived P-PSC average performance 11.3% (σ = 0.9) compares well to others reported in the literature for similar thickness of un-doped NiO HTL's of 10.6% (spin coated film, 40 nm) [10], 11.5% (30 nm) [38] and 10.2% (spray pyrolysis, 40 nm) [8].

4. Conclusions

We have demonstrated that FACVD is a viable process for deposition of continuous films of polycrystalline NiO suitable for efficient perovskite solar cells. This provides a low-cost production route to NiO HTL's via use of atmospheric, rather than low pressure with its high running costs, removal of the often required annealing stage and no need for environmentally detrimental organic solvents. Under the chosen FACVD deposition parameters the films became continuous at a thickness of ca. 36 nm resulting in efficient cell performance. The cells containing FACVD NiO with this thin film performed with comparable to better efficiency than those fabricated using an optimised spin coated NiO due to the strong improvement in the current density. The clear trend of NiO thickness against efficiency suggests that a slightly thicker film could improve the cell performance yet further.

Acknowledgements

HY and JLH received funding from the European Union's Horizon 2020 research and innovation programme under grant agreement No. 653296 (CHEOPS). SM and TW received funding from the UKRI Global Challenge Research Fund project, SUNRISE (EP/P032591/1). DR and TW acknowledge the financial support provided by the M2A that has been made possible through funding from the European Social Fund via the Welsh Government, the Engineering and Physical Sciences Research Council (EP/L015099/1) and TATA Steel.

XPS data collection was performed at the EPSRC National Facility for XPS ('HarwellXPS'), operated by Cardiff University and UCL, under contract No. PR16195. G. Parr, Salford Analytical Services provided the SEM images.

References

[1] D.B. Mitzi, C.A. Field, W.T.A. Harrison, A.M. Guloy, Conducting tin halides with a layered organic-based perovskite structure, Nature 369 (1994) 467-469.

[2] A. Kojima, K. Teshima, Y. Shirai, T. Miyasaka, Organometal Halide Perovskites as Visible-Light Sensitizers for Photovoltaic Cells. J.Am.Chem.Soc.131 (2009) 6050-6051.

[3] W.S. Yang, B.W. Park, E.H. Jung, N.J. Jeon, Y.C. Kim, D.U. Lee, S.S. Shin, J. Seo, E.K. Kim, J.H. Noh, S.I. Seok, Iodide management in formamidinium-lead-halide–based perovskite layers for efficient solar cells. Science 356 (2017) 1376-1379.

[4] https://www.oxfordpv.com/news/oxford-pv-perovskite-solar-cell-achieves-28-efficiency

[5] T. Leijtens, G.E. Eperon, S. Pathak, A. Abate, M.M. Lee, H. Snaith, Overcoming ultraviolet light instability of sensitized TiO_2 with meso-superstructured organometal tri-halide perovskite solar cells, Nat Commun. 4(2013) 2885-2893.

[6] Z.H. Liu ZH, A.L. Zhu, F.S. Cai, L.M. Tao, Y.H. Zhou, Z.X. Zhao, Q. Chen, Y.B. Cheng, H.P. Zhou, Nickel oxide nanoparticles for efficient hole transport in p-i-n and n-i-p perovskite solar cells, J.Mater.Chem. A, 5(2017) 6597-6605.

[7] M. Afzaal, H.M. Yates, A. Walter, S. Nicolay, Improved FTO/NiOx Interfaces for inverted planar triple cation perovskite solar cells. IEEE J Photovoltaics, 9 (2019) 1302-1308.

[8] W. Chen, Y. Wu, Y. Yue, J. Liu, W. Zhang, X. Yang, H. Chen, E. Bi, I. Ashraful, M. Grätzel, L. Han, Efficient and stable large-area perovskite solar cells with inorganic charge extraction layers. Science, 350 (2015) 944-948.

[9] H.S. Kim, J.Y. Seo, H. Xie, M. Lira-Cantu, S.M. Zakeeruddin, M. Grätzel, A. Hagfeldt, Effect of Cs-Incorporated NiO_x on the Performance of Perovskite Solar Cells. ACS Omega, 12 (2017) 9074-9079.

[10] X. Yin, Z. Yao, Q. Luo, X. Dai, Y. Zhou, Y. Zhang, Y. Zhou, S. Luo, J. Li, N. Wang, H. Lin, High Efficiency Inverted Planar Perovskite Solar Cells with Solution-Processed NiO_x Hole Contact, ACS Appl.Mater.Interfaces, 9 (2017) 2439-2448.

[11] M.Z. Sialvi, R.J. Mortimer, G.D. Wilcox, A.M. Teridi, T.S. Varley, K.G.U. Wijayantha and C.A. Kirk, Electrochromic and colorimetric properties of nickel (II) oxide thin films prepared by aerosol-assisted chemical vapor deposition, ACS Appl Mater Interfaces, 5 (2013) 5675-5682.

[12] J.W. Jung, C.-C. Chueh, A.K.-Y. Jen, A Low-Temperature, Solution-Processable, Cu-Doped Nickel Oxide Hole-Transporting Layer via the Combustion Method for High-Performance Thin-Film Perovskite Solar Cells, Adv.Mater., 27 (2015) 7874-7880.

[13] D.W. Sheel, L.A. Brook, H.M. Yates, Controlled nanostructured silver coated surfaces by atmospheric pressure Chemical Vapour Deposition, Chem.Vap.Deposition, 14 (2008) 14-24.

[14] M.A. Ehsan, M.A. Aziz, A. Rehman, A. S.Hakeem, M.A.A. Qasem, S.H.A. Ahmad, Aerosol-Assisted Chemical Vapor Deposition of Silver Thin Film Electrodes for Electrochemical Detection of 2-Nitrophenol, J.Electrochem.Soc., 165 (2018) B302-B309.

[15] H.M. Yates, L.A. Brook, D.W. Sheel, I.B. Ditta, A.Steele, H.A. Foster, The growth of copper oxides by FACVD, Thin Solid Films, 517 (2008) 517-521.

[16] I.A. Hassan, I.P. Parkin, S.P. Nair, C.J. Carmalt, Antimicrobial activity of copper and copper(I) oxide thin films deposited via aerosol-assisted CVD, J.Mater.Chem. B, 2 (2014) 2855-2860.

[17] S. Seo, I.J. Park, M. Kim, S. Lee, C. Bae, H.S. Jung, N-G. Park, J. Y. Kim, H. Shin, An ultra-thin, un-doped NiO hole transporting layer of highly efficient (16.4%) organic–inorganic hybrid perovskite solar cells, Nanoscale, 8 (2016) 11403-11412.

[18] H.-L. Chen, Y.-M. Lu and W.-S. Hwang, Characterization of sputtered NiO thin films, Surf.Coat.Technol., 198 (2005) 138-142.

[19] Z. Zhang, S. Chen, P. Li, H. Li, J. Wu, P. Hu, J. Wang, Aerosol-assisted chemical vapor deposition of ultra-thin CuO_x films as hole transport material for planar perovskite solar cells, Functional Mater.Lett., 11 (2018) 1850035.

[20] J. Troughton, K. Hooper, T.M. Watson, Humidity resistant fabrication of $CH_3NH_3PbI_3$ perovskite solar cells and modules, Nano Energy, 39 (2017) 60-68.

[21] S. Liu, R.Liu, Y.Chen, S. Ho, J.H. Kim, F. So, Nickel Oxide Hole Injection/Transport Layers for Efficient Solution-Processed Organic Light-Emitting Diodes, Chem.Mater. 26 (2014) 4528-3454.

[22] L.J. Tang, X. Chen, T.Y. Wen, S. Yang, J.J. Zhao, H.W. Qiao, Y. Hou, H.G. Yang, A Solution-Processed Transparent NiO Hole-Extraction Layer for High-Performance Inverted Perovskite Solar Cells, Chem.A, -Eur J., 24 (2018) 2845-2849.

[23] C. Zuo, A.D. Scully, D. Vak, W. Tan, X. Jiao, C.R. McNeill, D.Angmo, L.Ding and M. Gao, Self-Assembled 2D Perovskite Layers for Efficient Printable Solar Cells, Adv.Energy Mater., 9 (2019) 1803258.

[24] Z. Bi, Z. Liang, X. Xu, Z. Chai, H. Jin, D. Xu, J. Lia, M. Li, G. Xu, Fast preparation of uniform large grain size perovskite thin film in air condition via spray deposition method for high efficient planar solar cells, Sol.Energy Mater.Sol. Cells, 162 (2017) 13-20.

[25] F. De Rossi, J.A. Baker, D.Beynon, K.E.A. Hooper, S.M.P. Meroni, D.Williams, Z. Wei, A. Yasin, C. Charbonneau, E.H. Jewell, T.M. Watson, All Printable Perovskite Solar Modules with 198 cm^2 Active Area and Over 6% Efficiency, Adv.Mater.Technol. 3 (2018) 1800156.

[26] H.M.Yates, S.M.P. Meroni, D. Raptis, J.L. Hodgkinson, T.M. Watson, Flame Assisted Chemical Vapour Deposition NiO hole transport layers for mesoporous carbon perovskite cells, J.Mater.Chem.C., 7 (2019) 13235–13242.

[27] J.L. Hodgkinson, H.M. Yates, NiO_x via Flame Assisted CVD as a route to stable, low cost, large area, hole transport layers for perovskite solar cells, Proc. PVSAT 14, The Solar Energy Soc. London UK, April 2018. pp81-84.

[28] https://imagej.nih.gov/ij/download.html

[29] B.D. Cullity, Elements of X-Ray Diffraction, 2nd Edition, Addison-Wesley, Reading, Mass, 1978.

[30] [a] C. Friesen, S.C. Seel, C.V. Thompson, Reversible stress changes at all stages of Volmer–Weber film growth, J.Appl.Phys., 95 (2004) 1011-1020. [b] M. Ohring, 'Materials Science of Thin Films', Academic Press, 2002.

[31] M.J. Davis, G. Benito, D.W. Sheel and M.E. Pemble, Growth of thin films of molybdenum and tungsten oxides by combustion CVD using aqueous precursor solutions, Chem.Vap.Deposition, 10 (2004) 29-34.

[32] M. Afzaal, H.M. Yates, J.L. Hodgkinson, Translation effects on the properties of FTO thin films by in-line atmospheric pressure CVD, Coatings, 6 (2016) 43-52.

[33] Chastain J, King RC. Handbook of X – Ray Photoelectron Spectroscopy, Physical Electronic Inc, New York, 1995.

[34] D.T. Clarke, T. Fok, G.G. Roberts, R.W. Sykes, An investigation by electron spectroscopy for chemical analysis of chemical treatments of the (100) surface of n-type InP epitaxial layers for Langmuir film deposition, Thin Solid Films, 70 (1980) 261-283.

[35] J.Y. Zhou, J.L. Bai, H. Zhou, Z.Y. Yang, X.Y. Gu, B.Y. Huang, C.H. Zhou, L. Cairang, G.Z. Sun, Z.X. Zhang, X.J. Pan, E.Q. Xie, Gas sensing enhancing mechanism via doping-induced oxygen vacancies for gas sensors based on indium tin oxide nanotubes, Sensors Actuators B., 265 (2018) 273-284.

[36] E. Turgut, O. Coban, S. Santa, S. Tuzemen, M. Yildirm, Oxygen partial pressure effects on the RF sputtered p-type NiO hydrogen gas sensors, Appl.Surf.Sci.,435 (2019) 880-885.

[37] A.G. Marrani, V. Novelli, S. Sheehan, D.P. Dowling, D. Dini, Probing the Redox States at the Surface of Electroactive Nanoporous NiO Thin Films, ACS Appl.Mater. Interfaces, 6 (2014) 143-152.

[38] A.F. Curley, S.D. Jackson, J.N. O'Shea, M.W. Roberts, The formation and characterisation of Ni^{3+} - an X-ray photoelectron spectroscopic investigation of potassium-doped Ni(110)-O, Surf.Sci.Lett., 440 (1999) L868-874.

[39] N.D. Hoa, P.V. Tong, C.M. Hung, N.V. Duy, N.V. Hieu, Urea mediated synthesis of $Ni(OH)_2$ nanowires and their conversion into NiO nanostructure for hydrogen gas-sensing application, Intl.J.Hyd.Ener., 43 (2018) 9446-9453.

[40] A.P. Grosvenor, M.C. Biesinger, R.St.C. Smart, N.S. McIntyre, New interpretations of XPS spectra of nickel metal and oxides, Surf.Sci., 600 (2006) 1771-1779.

[41] J.Tang, D. Jiao, L. Zhang, X. Zhang, X. Xu, C. Yao, J. Wu, Z. Lan, High-performance inverted planar perovskite solar cells based on efficient hole-transporting layers from well-crystalline NiO nanocrystals, Solar Energy, 161 (2018) 100-108.

[42] D.S. Saranin, V.N. Mazov, L.O. Luchnikov, D.A. Lypenko, P.A. Gostishev, D.S. Muratov, D.A. Podgorny, D.M. Migunov, S.I. Didenko, M.N. Orlova, D.V. Kuznetsov, A.R. Tameev, A. Di Carlo, Tris(ethylene diamine) nickel acetate as a promising precursor for hole transport layer in planar structured perovskite solar cells, J.Mater. Chem.C., 6 (2018) 6179-6186.

[43] Y. Bai, H.N. Chen, S. Xiao, Q.F. Xue, T. Zhang, Z.L. Zhu, Q. Li, C. Hu, Y. Yang, Z.C. Hu, F. Huang, K.S. Wong, H.L. Yip, S.H. Yang, Effects of a molecular monolayer modification of NiO nanocrystal layer surfaces on perovskite crystallization and interface contact toward faster hole extraction and higher photovoltaic performance, Adv.Funct.Mater. 26 (2016) 2950-2958.

[44] Y. Chen, L. Zhang, Y. Zhang, H. Gao, H. Yan, Large-area perovskite solar cells – a review of recent progress and issues, RSC Adv., 8 (2018) 10489-10508.

List of figures captions

Figure 1. SEM images of NiO with a) 10 pass, b) 20 pass, c) 50 pass (standard flame), d) 50 pass (lean flame)

Figure 2. Graph showing the mean size and separation of the NiO islands.

Figure 3. X-ray diffraction of a) ITO as supplied, b) After 50 passes under a standard flame, c) After 50 passes under a lean flame.

Figure 4. XRD of a) bare ITO substrate, b) 12 passes NiO on ITO, c) 50 passes NiO on ITO, d) 60 passes NiO

Figure 5. SEM surface images. a) ITO, b) 50 passes NiO on ITO, c) 50 passes NiO on glass.

Figure 6. AFM images (size 5 μm x 5 μm) a) ITO substrate, b) 50 passes NiO on ITO, c) 50 passes NiO on glass, d) Histogram to compare the spread in feature height on deposition of NiO.

Figure 7. High resolution XPS scans of In 3d a) bare ITO substrate, b) 8 passes NiO, c) 12 passes, d) 50 passes. Graph shows the shift in In $3d_{5/2}$ position with the amount of NiO deposited. The position for the as received and flame treated ITO are placed at the '60 pass' position.

Figure 8. High resolution XPS Ni 2p scan for a) 50 passes NiO deposited directly on glass, b) 50 passes NiO on ITO, c) 12 passes NiO on ITO

Figure 9. Statistical box plots for planar MAPI perovskite cells on ITO

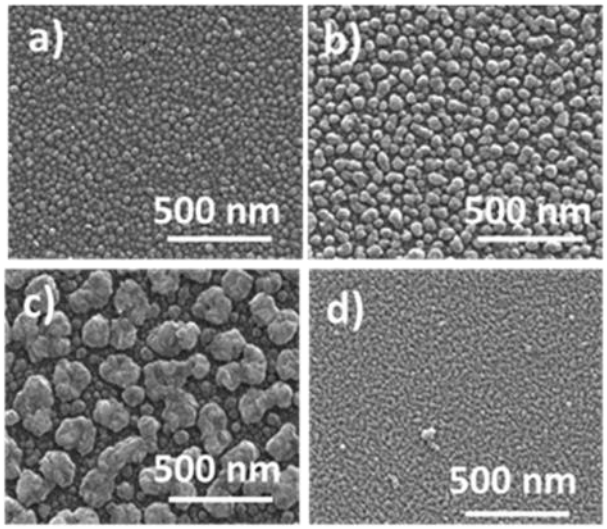

Fig.1

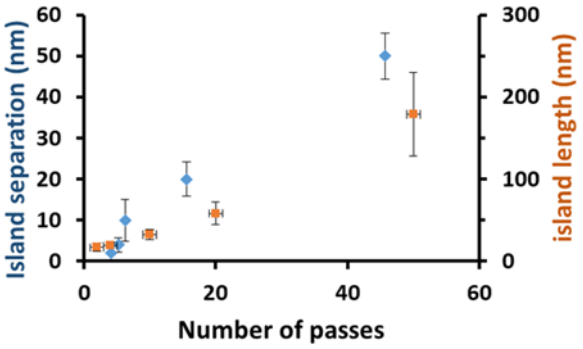

Fig.2

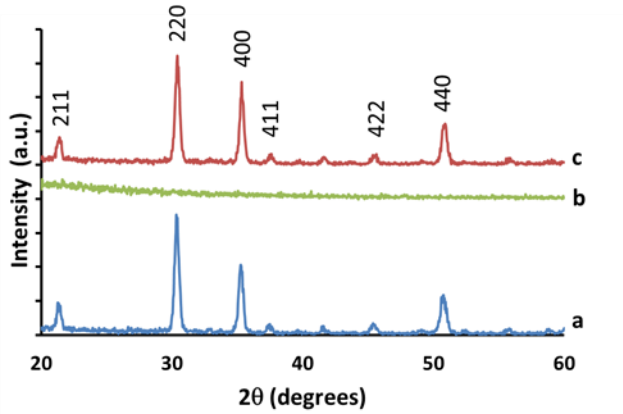

Fig.3

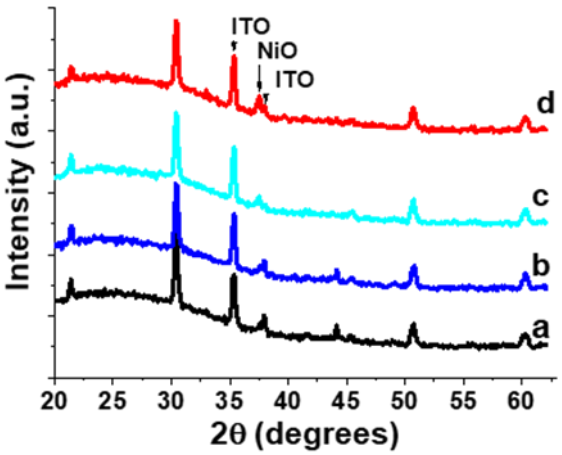

Fig.4

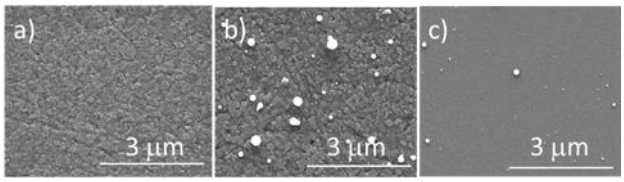

Fig.5

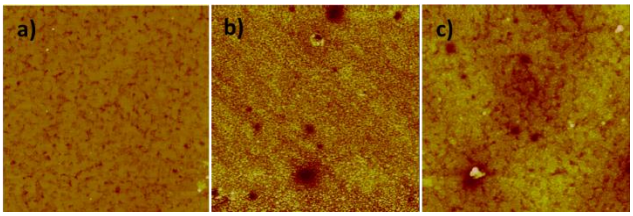

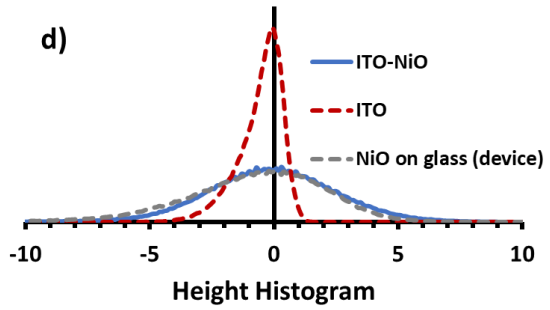

Fig.6

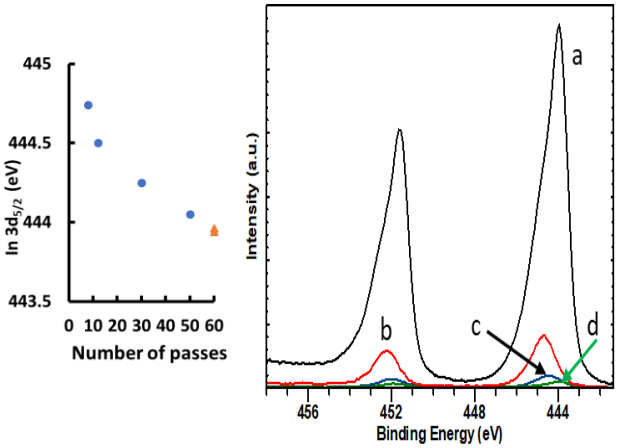

Fig.7

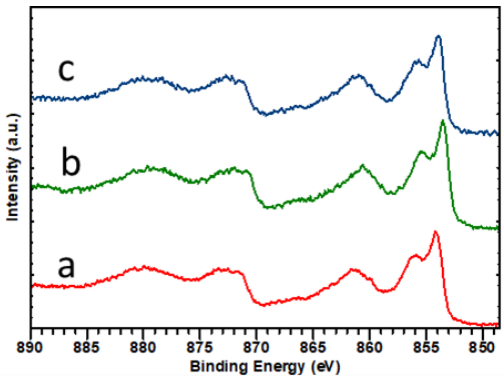

Fig.8

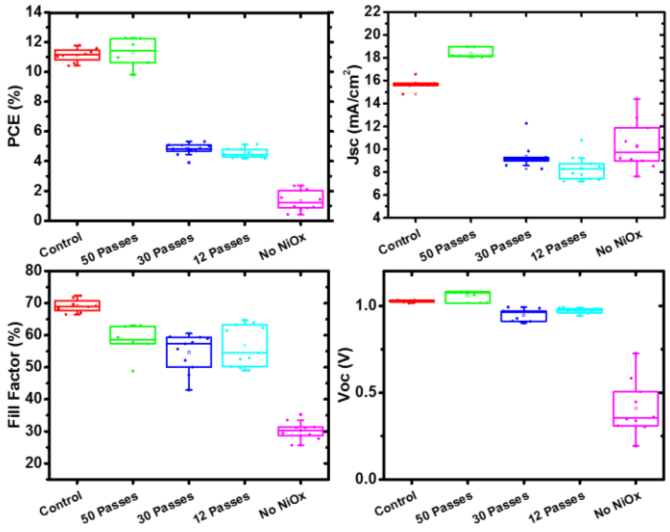

Fig.9

Flame Assisted Chemical Vapour Deposition NiO hole transport layers for planar perovskite cells

Heather M. Yates[1], John L. Hodgkinson[1], Simone. M.P. Meroni[2], David Richards[2] and Trystan M. Watson[2]

[1]Materials and Physics Research Centre, University of Salford, Manchester, M5 4WT, UK.
[2]SPECIFIC, Swansea University, Bay Campus, Fabian Way, Crymlyn Burrows, Swansea, SA1 8EN, Wales UK

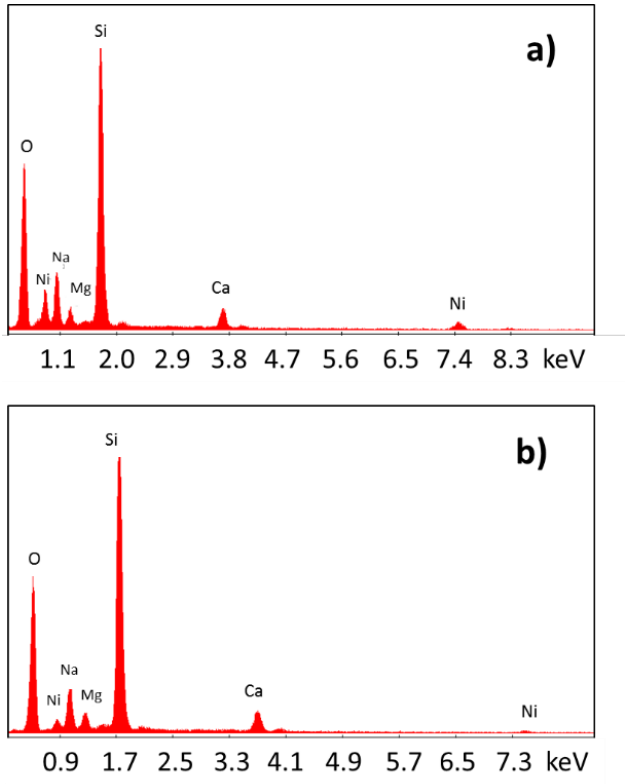

Fig.S1, EDAX of NiO film a) large particles, b) small particles

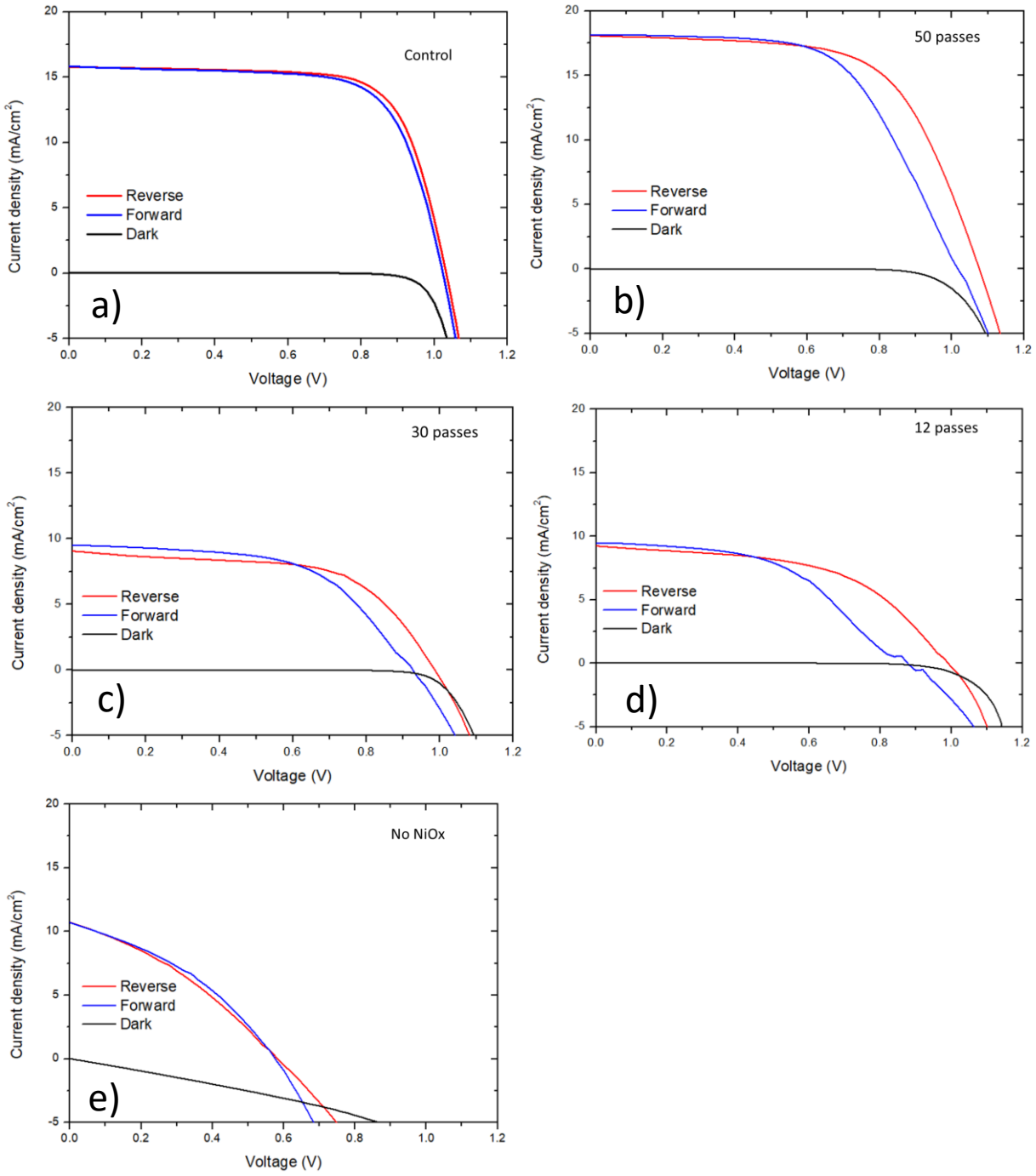

Fig.S2, JV curves for a) control cell (spin coated NiO), b) cell using 50 passes FACVD NiO, c) 30 passes NiO, d) 12 passes NiO, e) 'no NiO'